Supporting Information

Direct Observation of the Reduction of Aryl Halides by Photoexcited Perylene Diimide Radical Anion

Charles J. Zeman IV[†,#], Soojin Kim[‡,#], Fang Zhang[§*] and Kirk S. Schanze[‡,*]

[†] Department of Chemistry, University of Florida, Gainesville, FL, 32611

[‡] Department of Chemistry, University of Texas at San Antonio, One UTSA Circle, San Antonio, TX 78249

[§] The Education Ministry Key Laboratory of Resource Chemistry, Shanghai Normal University, Shanghai 200234, China

Corresponding Author

* E-mail: kirk.schanze@utsa.edu

CONTENTS

1. EXPERIMENTAL METHODS

Materials. N,N'-Bis(2,6-diisopropylphenyl)-3,4,9,10-perylenetetracarboxylic diimide (PDI) was purchased from TCI. Tetrakis(dimethylamino)ethylene (TDAE) was purchased from Sigma Aldrich. All Aryl halides and quenchers were commercially available and used without further purification. DMF was purified and dried using an MBraun MB-SPS-800 solvent purification system and kept in an inert atmosphere (N_2) glove box.

General Procedure for Sample Preparation. Solvent was purged with N_2 for 30 min before transferring to an inert atmosphere glove box where all sample preparation was carried out. Samples were prepared by adding aliquots of a specified concentration of quencher to a 60 μM solution of PDI radical anion that was generated by thermal reduction with TDAE in dry DMF. The samples were mixed in a 2 mm path length quartz cuvette which was covered with aluminum foil to prevent light exposure. For photoinduced electron transfer studies and thermal reactivity under dark conditions, an aliquot of quencher in DMF was added to the premixed solution of PDI and TDAE. Before removal from the glovebox, all samples were sealed by a rubber septum, Teflon tape, and parafilm.

UV-Visible Absorption Spectroscopy. Steady-state electronic absorption spectra were collected using a Shimadzu UV-1800 dual-beam spectrophotometer referenced to DMF. Samples were kept isolated from light by aluminum foil prior to data collection. Special care was taken to ensure that these samples were never exposed to light or oxygen. For monitoring spectral change over time under dark conditions, spectra were collected repeatedly over the course of one hour.

Ultrafast Transient Absorption Spectroscopy. Sub-picosecond transient absorption spectroscopy was made possible using a pump-probe technique with the fundamental 800 nm light as generated by a Coherent Astrella Ti:sapphire Amplifier (120 fs, 1 kHz) and splitting it into two beams. Sufficient power was dumped for both beams so as to not induce damage to any optics. The first beam was directed through an optical parametric amplifier as supplied by Coherent where the wavelength was tuned to 700 nm for pumping. Subsequently, both beams were guided into a HELIOS Femtosecond Transient Absorption Spectrometer (Ultrafast Systems, LLC) where the 700 nm pump passed through a chopper, halving its repetition rate, and a neutral density filter that was used to adjust the average power to 0.15 mW (150 nJ/pulse).

The second beam was passed through a digitally-controlled delay stage with a maximum range of 8 ns followed by a sapphire plate for generation of the white light continuum used for probing. The two beams overlap at the sample position with their respective electronic polarizations at the magic angle. An absorption spectrum with and without pumping was collected using a fiber-coupled spectrometer at several (>100) time delays to produce an array of absorption difference spectra. Chirp, time-zero, and solvent response corrections were employed using the software supplied by Ultrafast Systems where global analysis was done by reconstructing the spectra from two principal component eigenspectra with their associated lifetimes. Corrected and normalized changes in ΔO.D. with time at 460 nm were taken from the difference spectra and fit to exponential decays using the proprietary data analysis software from OriginLab Corporation (version 8.5) for all concentrations of each quencher.

2. REHM-WELLER ANALYSIS

The experimental data set was empirically fitted using the Rehm-Weller equation,[1]

$$k_q^{ET} = \frac{k_d}{1+\exp\left(\frac{\Delta G}{RT}\right)+\frac{k_{-d}}{k_{ET}^0}\exp\left\{\frac{\Delta G+\frac{\Delta G^{\ddagger}(0)}{\ln 2}\ln\left[1+\exp\left(-\frac{\Delta G \ln 2}{\Delta G^{\ddagger}(0)}\right)\right]}{RT}\right\}} \quad \text{(S-1)}$$

where k_q^{ET} is the quenching rate by electron transfer for a given aryl compound taken from Stern-Volmer analysis, k_d is the rate of diffusion, k_{-d} is the dissociation rate of the encounter complex, k^o_{ET} is the Arrhenius preexponential factor, $\Delta G^{\neq}(0)$ is the standard free energy of activation for $\Delta G = 0$ (note that $\Delta G^{\neq}(0) = \lambda/4$, where λ is the total reorganization energy). ΔG is the free energy for electron transfer given by,

$$\Delta G = E^o(*PDI^{-\bullet}/PDI) - E^o(ArX/ArX^{-}) \quad \text{(S-2)}$$

where $E^o(*PDI^{-\bullet}/PDI)$ is the oxidation potential of the doublet excited state of the anion, $*PDI^{-\bullet}$, and $E^o(ArX/ArX^{-})$ is the reduction potential of the aryl quencher taken from the literature. For the fit shown in Fig. 3b, the following values were used: $k_d = 1.80 \times 10^{10}$ $M^{-1}s^{-1}$, $k_{-d} = 3.00 \times 10^{10}$ s^{-1}, and $k^o_{ET} = 5.0 \times 10^{11}$ s^{-1}. The following procedure was used to fit the experimental data to eq. S-2. First, the Arrhenius preexponential factor (k^o_{ET}) was fixed to a value taken from the literature, and is consistent with an outer-sphere electron transfer process.[1-3] Then the diffusion and dissociation rates (k_d and k_{-d}) were adjusted so as to obtain the best fit for the data at maximum rate (i.e. the high driving force, diffusion-controlled plateau region). The values used are consistent with what is expected according to previous work.[1-3] Finally, holding the aforementioned k^o_{ET}, k_d and k_{-d} values constant, the values of $\Delta G^{\neq}(0)$ and $E^o(*PDI^{-\bullet}/PDI)$ were optimized using an iterative reduced X^2 procedure where X is the difference between experimental data points and the fit curve. This procedure identified values of $\Delta G^{\neq}(0) = 0.21$ eV ($\lambda = 0.84$ eV) and $E^o(*PDI^{-\bullet}/PDI) = -1.87$ V.

3. PHOTOREDUCTION OF PDI$^{-\bullet}$ WITH QUENCHER

3.1 4-Nitrobenzaldehyde

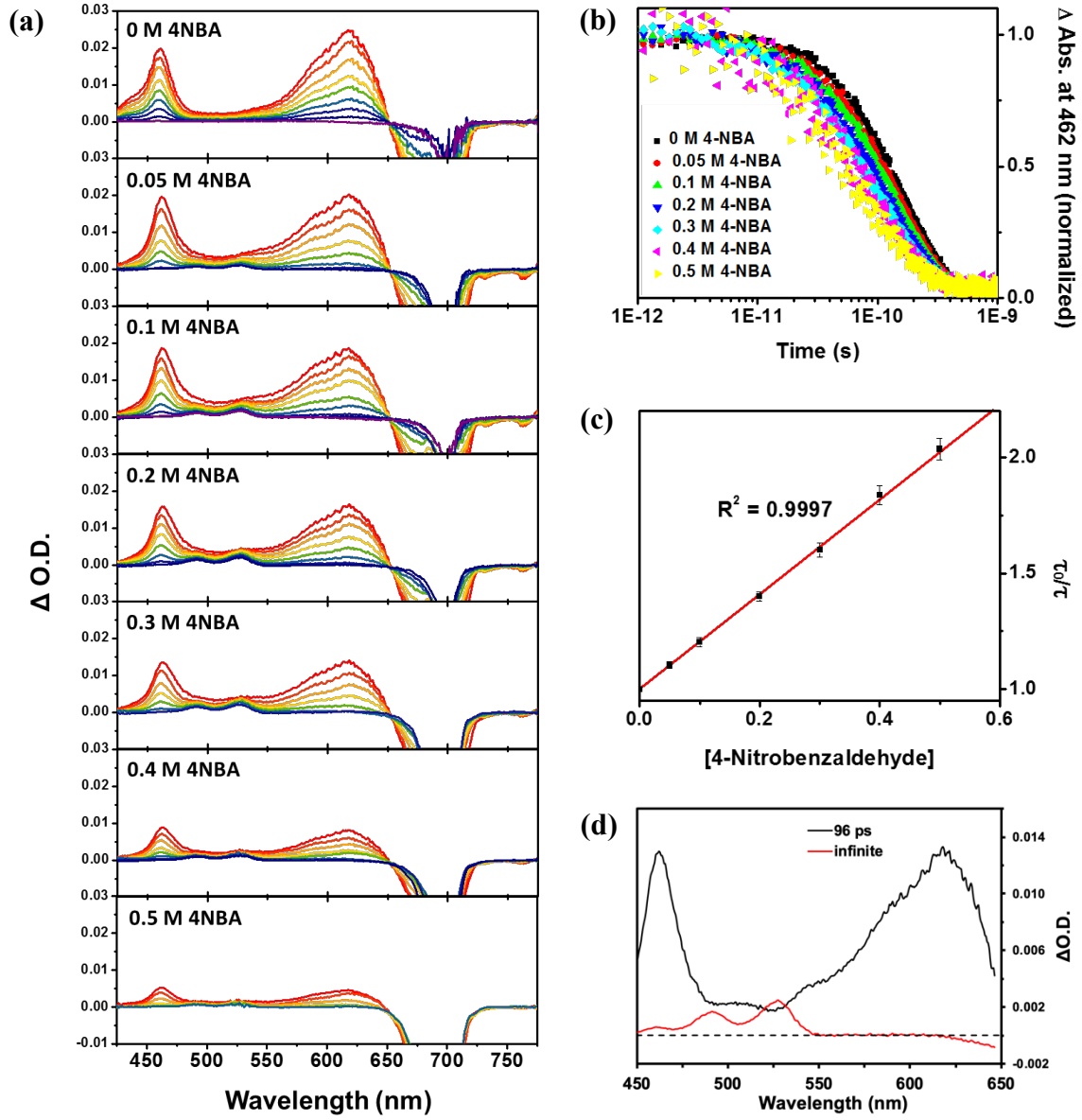

Figure S1. (a) Transient absorption spectra of 60 μM PDI$^{-\bullet}$ with 0 ~ 0.5 M of 4-nitrobenzaldehyde in DMF. (b) Normalized kinetic traces at 462 nm of 60 μM PDI$^{-\bullet}$ with various concentration of 4-nitrobenzaldehyde in DMF. (c) Stern-Volmer plot for the lifetime quenching of PDI$^{-\bullet}$ with various concentration of 4-nitrobenzaldehyde in DMF. (d) Principal component spectral/kinetic analysis of transient absorption data for 0.3 M 4NBA. Shown are the eigenspectra that correspond to *PDI$^{-\bullet}$ (96 ps component) and the electron transfer products (infinite time). Note that the product eigenspectrum (infinite) corresponds to neutral PDI; absorption that can be attributed to 4NBA$^{-\bullet}$ is not resolved. This is likely due to the relatively low molar absorptivity of the latter in the visible region.[4]

3.2 3-Nitrobenzaldehyde

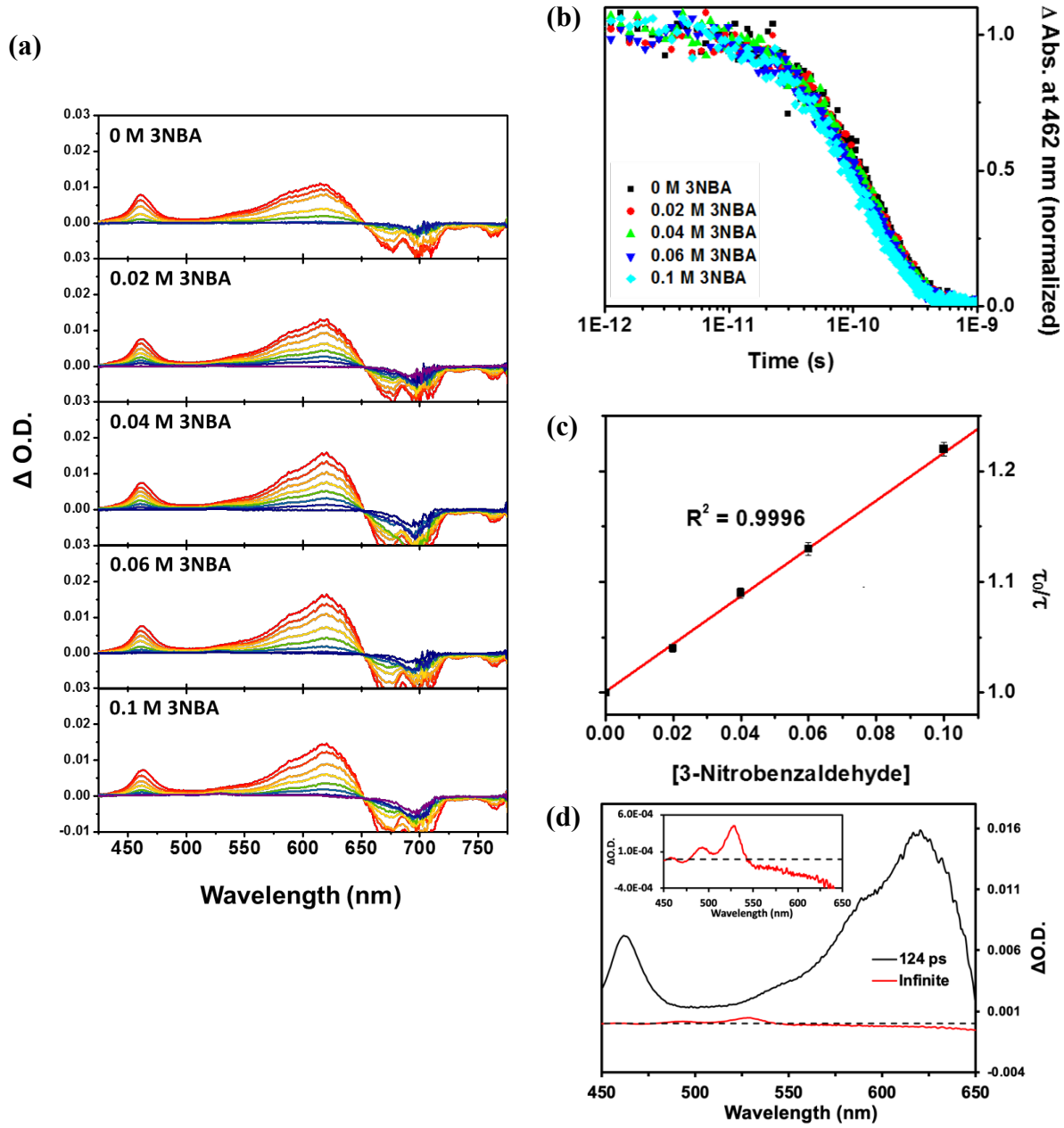

Figure S2. (a) Transient absorption spectra of 60 μM $PDI^{-\bullet}$ with 0 ~ 0.1 M of 3-nitrobenzaldehyde in DMF. (b) Normalized kinetic traces at 462 nm of 60 μM $PDI^{-\bullet}$ with various concentration of 3-nitrobenzaldehyde in DMF. (c) Stern-Volmer plot for the lifetime quenching of $PDI^{-\bullet}$ with various concentration of 3-nitrobenzaldehyde in DMF. (d) Principal component spectral/kinetic analysis of transient absorption data for 0.1 M 3NBA. Shown are the eigenspectra that correspond to $*PDI^{-\bullet}$ (124 ps component) and the electron transfer products (infinite time). Note that the product eigenspectrum (infinite) corresponds to neutral PDI; absorption that can be attributed to $3NBA^{-\bullet}$ is not resolved. This is likely due to the relatively low molar absorptivity of the latter in the visible region.[4]

3.3 Nitrobenzene

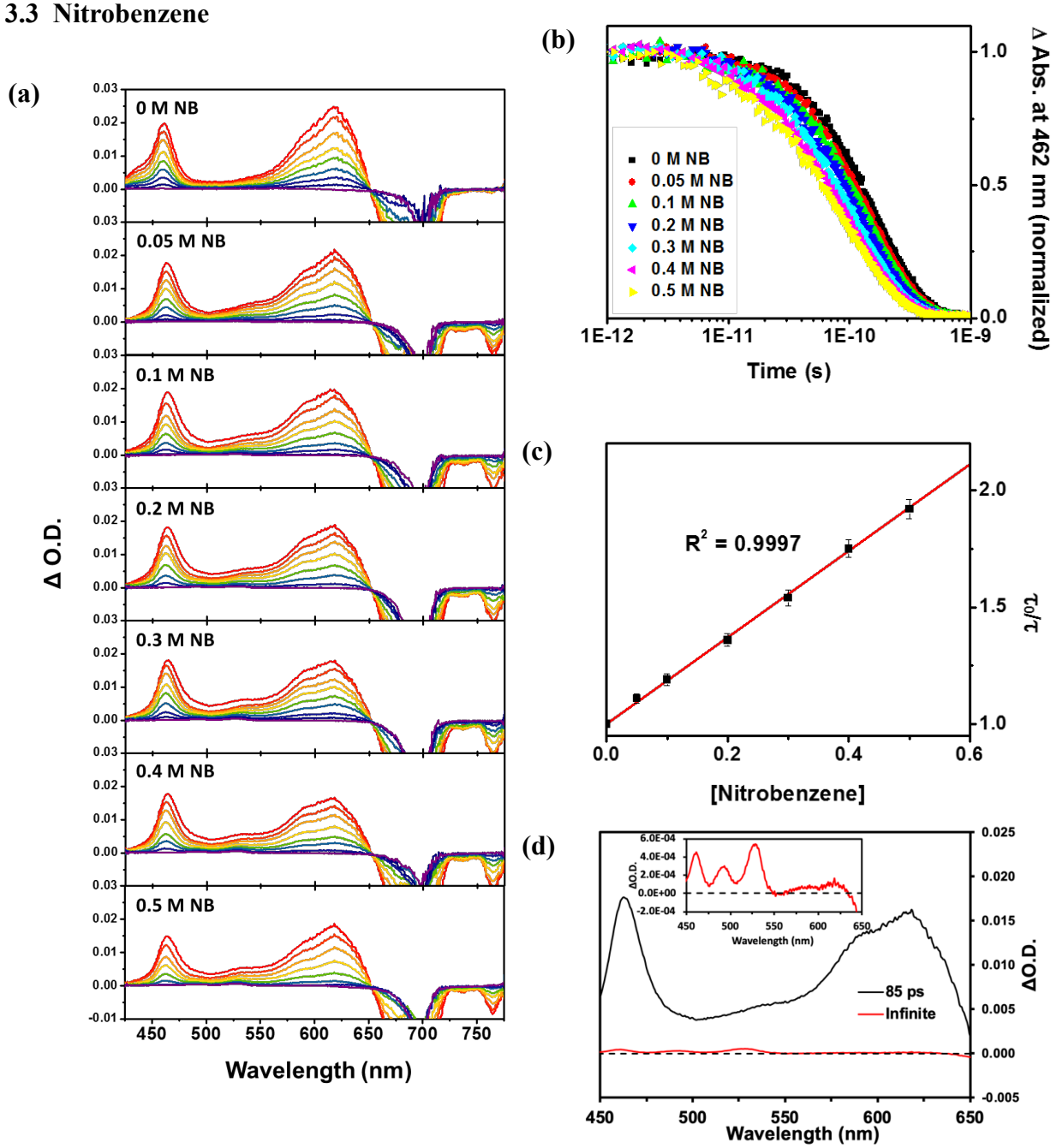

Figure S3. (a) Transient absorption spectra of 60 μM $PDI^{-\bullet}$ with 0 ~ 0.5 M of nitrobenzene in DMF. (b) Normalized kinetic traces at 462 nm of 60 μM $PDI^{-\bullet}$ with various concentration of nitrobenzene in DMF. (c) Stern-Volmer plot for the lifetime quenching of $PDI^{-\bullet}$ with various concentration of nitrobenzene in DMF. (d) Principal component spectral/kinetic analysis of transient absorption data for 0.4 M NB. Shown are the eigenspectra that correspond to $*PDI^{-\bullet}$ (85 ps component) and the electron transfer products (infinite time). Note that the product eigenspectrum (infinite) corresponds to neutral PDI; absorption that can be attributed to $NB^{-\bullet}$ is not resolved. This is likely due to the relatively low molar absorptivity of the latter in the visible region.[4] The peak at ~460 in inset is $*PDI^{-\bullet}$ absorbance that is unresolved by the analysis.

3.4 4-Nitroanisole

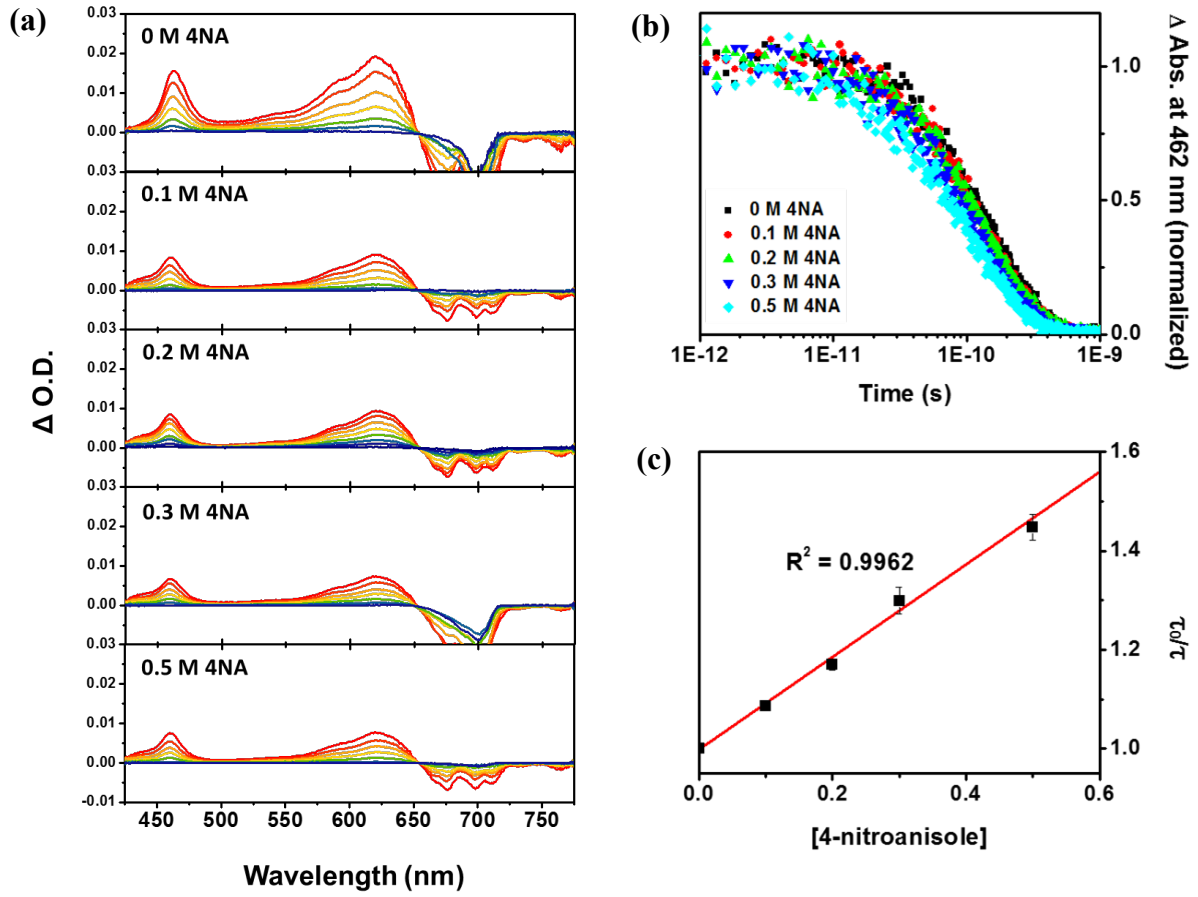

Figure S4. (a) Transient absorption spectra of 60 μM $PDI^{-\bullet}$ with 0 ~ 0.5 M of 4-nitroanisole in DMF. (b) Normalized kinetic traces at 462 nm of 60 μM $PDI^{-\bullet}$ with various concentration of 4-nitroanisole in DMF. (c) Stern-Volmer plot for the lifetime quenching of $PDI^{-\bullet}$ with various concentration of 4-nitroanisole in DMF.

3.5 2-Bromobenzaldehyde

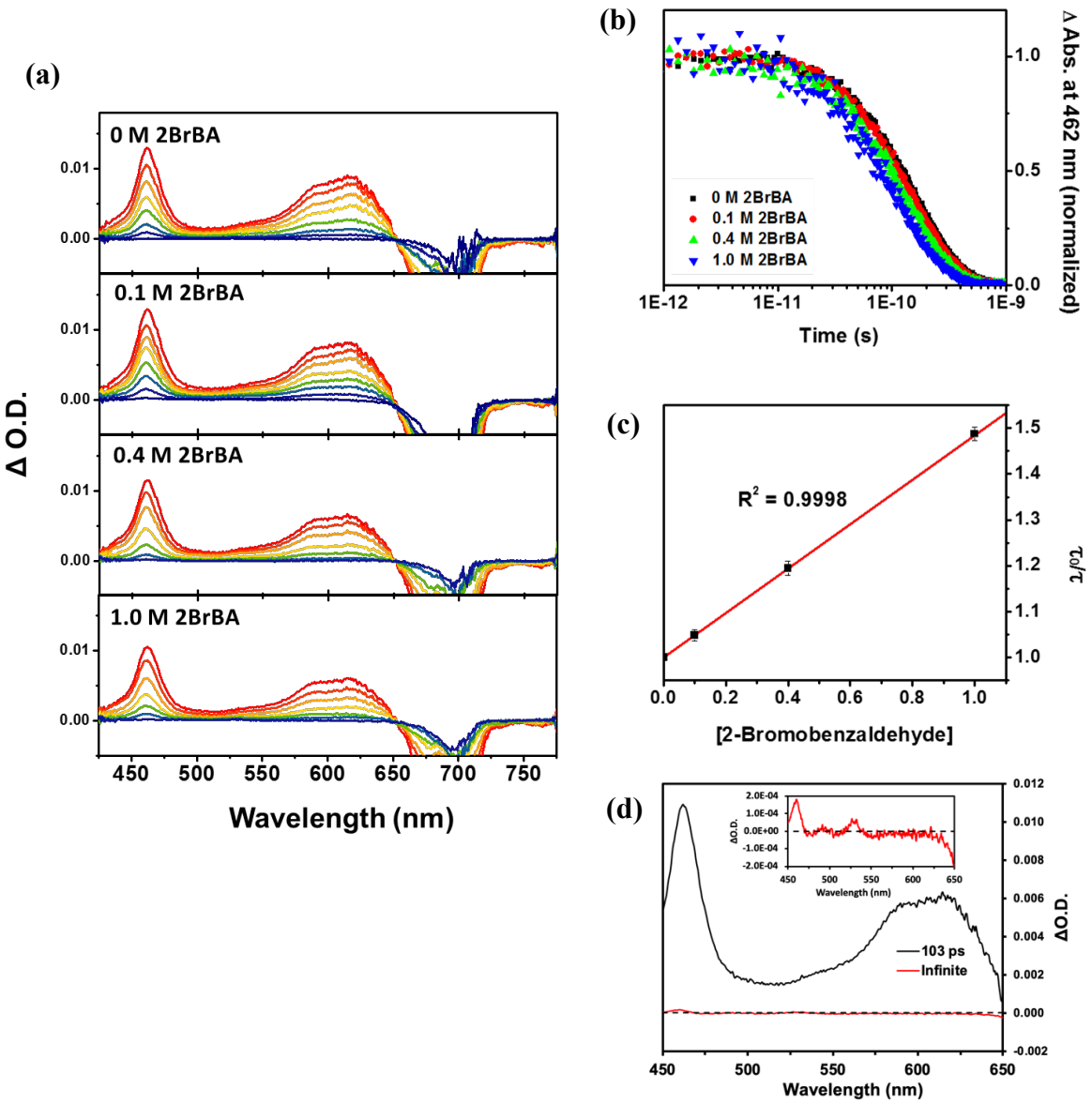

Figure S5. (a) Transient absorption spectra of 60 μM $PDI^{-\bullet}$ with 0 ~ 1.0 M of 2-bromobenzaldehyde in DMF. (b) Normalized kinetic traces at 462 nm of 60 μM $PDI^{-\bullet}$ with various concentration of 2-bromobenzaldehyde in DMF. (c) Stern-Volmer plot for the lifetime quenching of $PDI^{-\bullet}$ with various concentration of 2-bromobenzaldehyde in DMF. (d) Principal component spectral/kinetic analysis of transient absorption data for 1.0 M 2BrBA. Shown are the eigenspectra that correspond to $*PDI^{-\bullet}$ (103 ps component) and the electron transfer products (infinite time). Note that the product eigenspectrum (infinite) corresponds to neutral PDI; absorption that can be attributed to $2BrBA^{-\bullet}$ is not resolved. This is likely due to the relatively low molar absorptivity of the latter in the visible region.[4] The peak at ~460 in inset is $*PDI^{-\bullet}$ absorbance that is unresolved by the analysis.

3.6 4-Iodobenzaldehyde

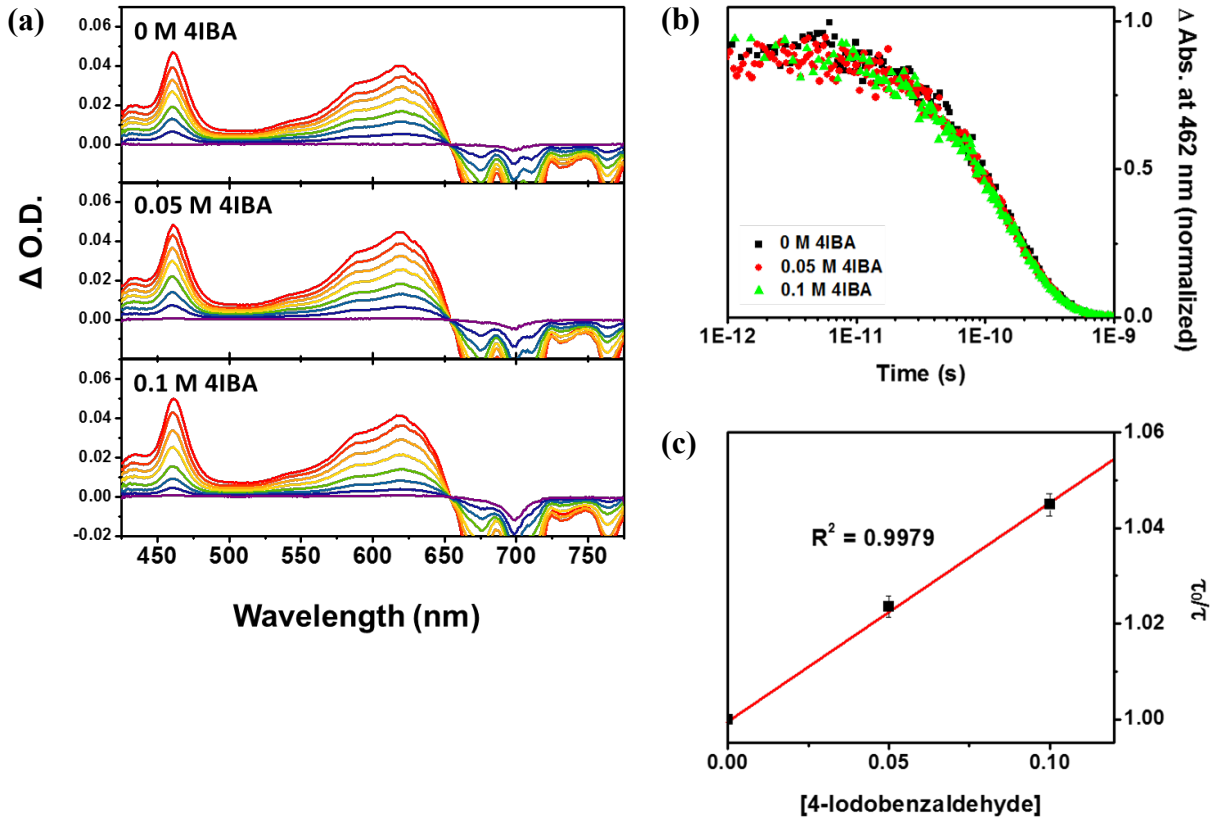

Figure S6. (a) Transient absorption spectra of 60 μM $PDI^{-\bullet}$ with 0 ~ 0.1 M of 4-iodobenzaldehyde in DMF. (b) Normalized kinetic traces at 462 nm of 60 μM $PDI^{-\bullet}$ with various concentration of 4-iodobenzaldehyde in DMF. (c) Stern-Volmer plot for the lifetime quenching of $PDI^{-\bullet}$ with various concentration of 4-iodobenzaldehyde in DMF.

3.7 3-Iodobenzaldehyde

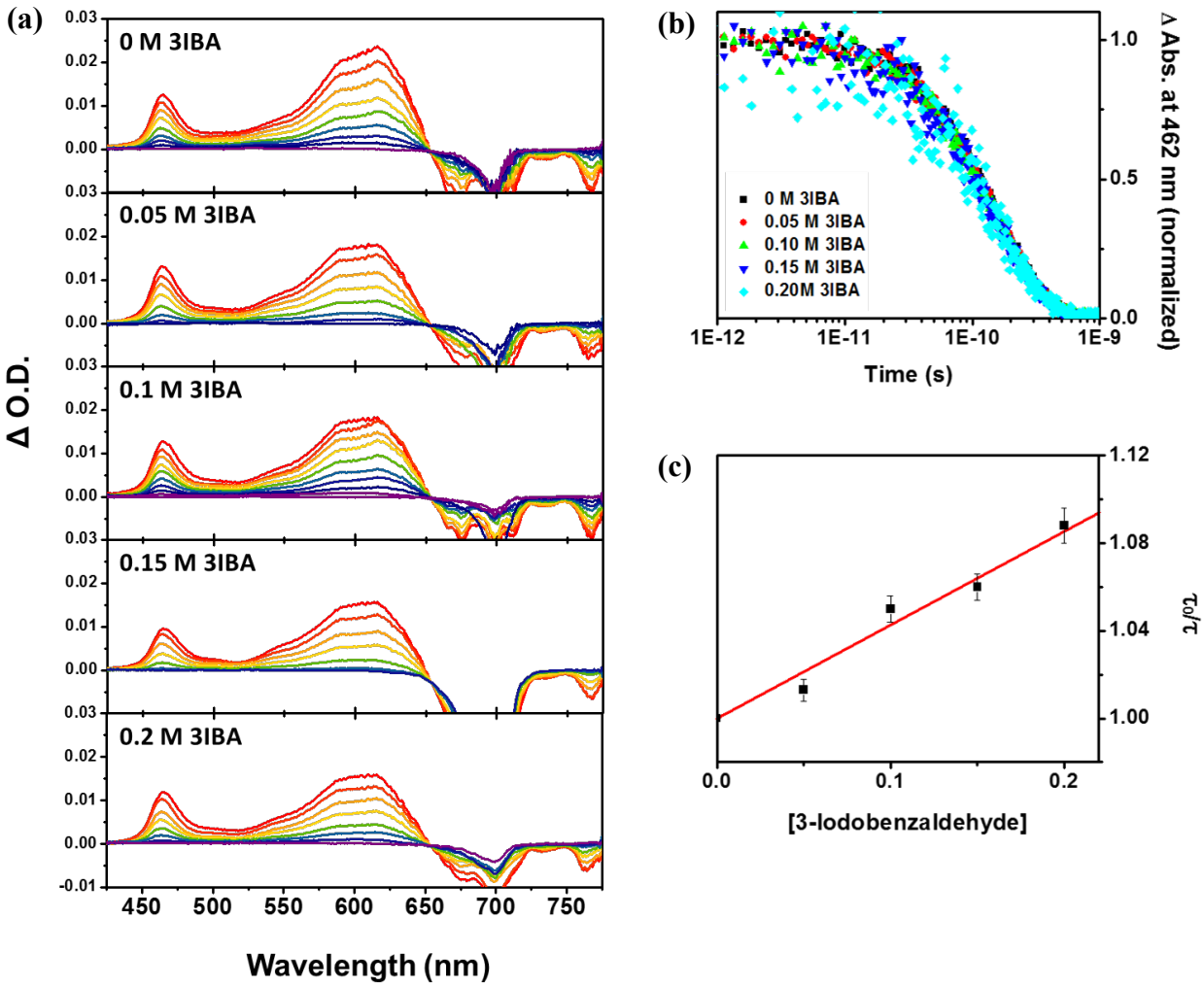

Figure S7. (a) Transient absorption spectra of 60 μM $PDI^{-\bullet}$ with 0 ~ 0.2 M of 3-iodobenzaldehyde in DMF. (b) Normalized kinetic traces at 462 nm of 60 μM $PDI^{-\bullet}$ with various concentration of 3-iodobenzaldehyde in DMF. (c) Stern-Volmer plot for the lifetime quenching of $PDI^{-\bullet}$ with various concentration of 3-iodobenzaldehyde in DMF.

3.8 4-Bromobenzaldehyde

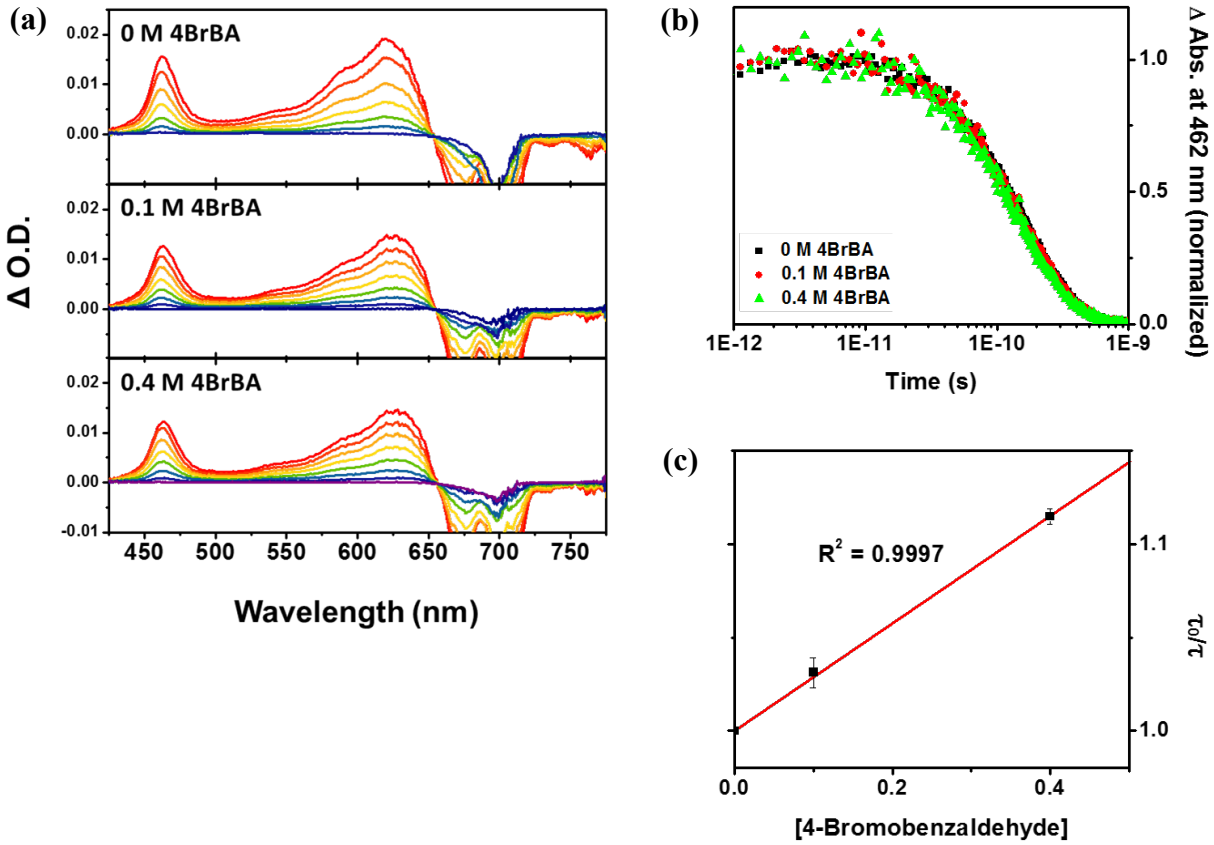

Figure S8. (a) Transient absorption spectra of 60 μM $PDI^{-\bullet}$ with 0 ~ 0.4 M of 4-bromobenzaldehyde in DMF. (b) Normalized kinetic traces at 462 nm of 60 μM $PDI^{-\bullet}$ with various concentration of 4-bromobenzaldehyde in DMF. (c) Stern-Volmer plot for the lifetime quenching of $PDI^{-\bullet}$ with various concentration of 4-bromobenzaldehyde in DMF.

3.9 1,4-Dinitrobenzene

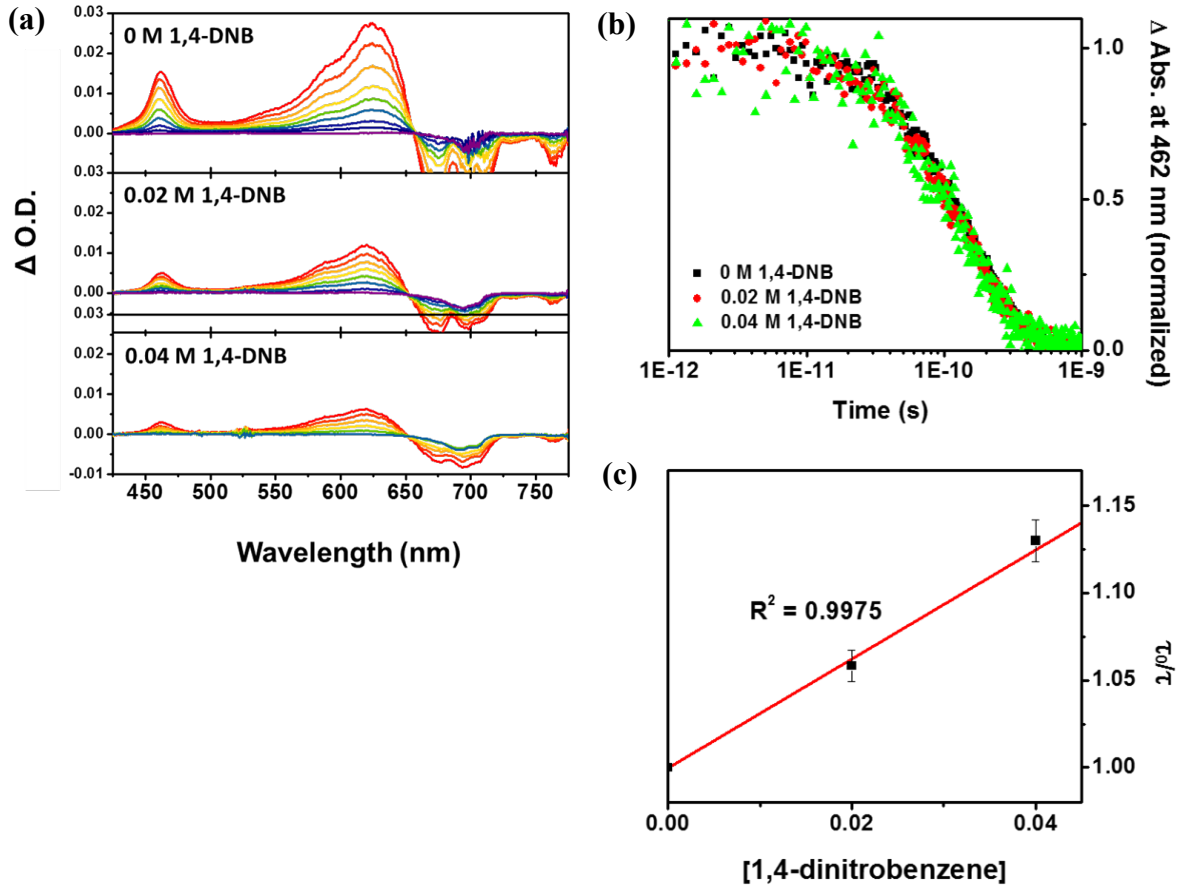

Figure S9. (a) Transient absorption spectra of 60 μM $PDI^{-\bullet}$ with 0 ~ 0.04 M of 1,4-dinitrobenzene in DMF. (b) Normalized kinetic traces at 462 nm of 60 μM $PDI^{-\bullet}$ with various concentration of 1,4-dinitrobenzene in DMF. (c) Stern-Volmer plot for the lifetime quenching of $PDI^{-\bullet}$ with various concentration of 1,4-dinitrobenzene in DMF.

3.10 4-Bromoacetophenone

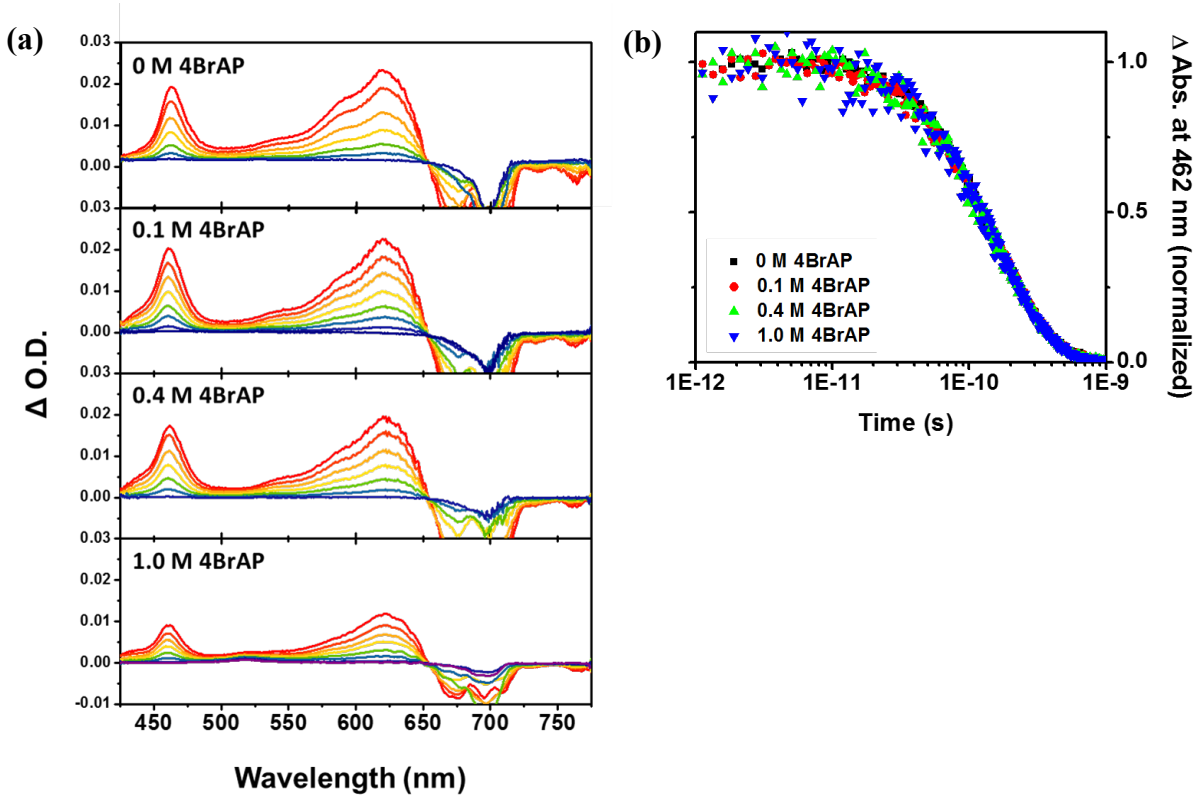

Figure S10. (a) Transient absorption spectra of 60 μM $PDI^{-\bullet}$ with 0 ~ 1.0 M of 4-bromoacetophenone in DMF. (b) Normalized kinetic traces at 462 nm of 60 μM $PDI^{-\bullet}$ with various concentration of 4-bromoacetophenone in DMF.

3.11 4-Chloroacetophenone

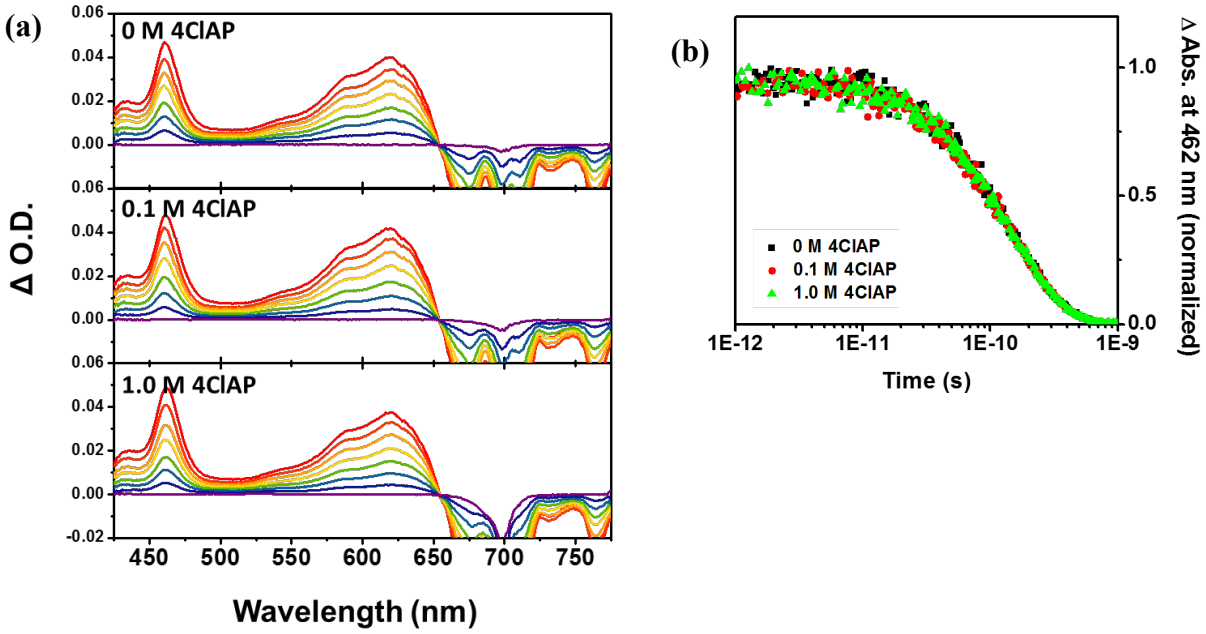

Figure S11. (a) Transient absorption spectra of 60 μM $PDI^{\bullet-}$ 0 ~ 1.0 M of 4-chloroacetophenone in DMF. (b) Normalized kinetic traces at 462 nm of 60 μM $PDI^{\bullet-}$ with various concentration of 4-chloroacetophenone in DMF. Note that the Stern-Volmer plot is not shown since there is no quenching observed up to 1.0 M concentration.

3.12 4-Bromoanisole

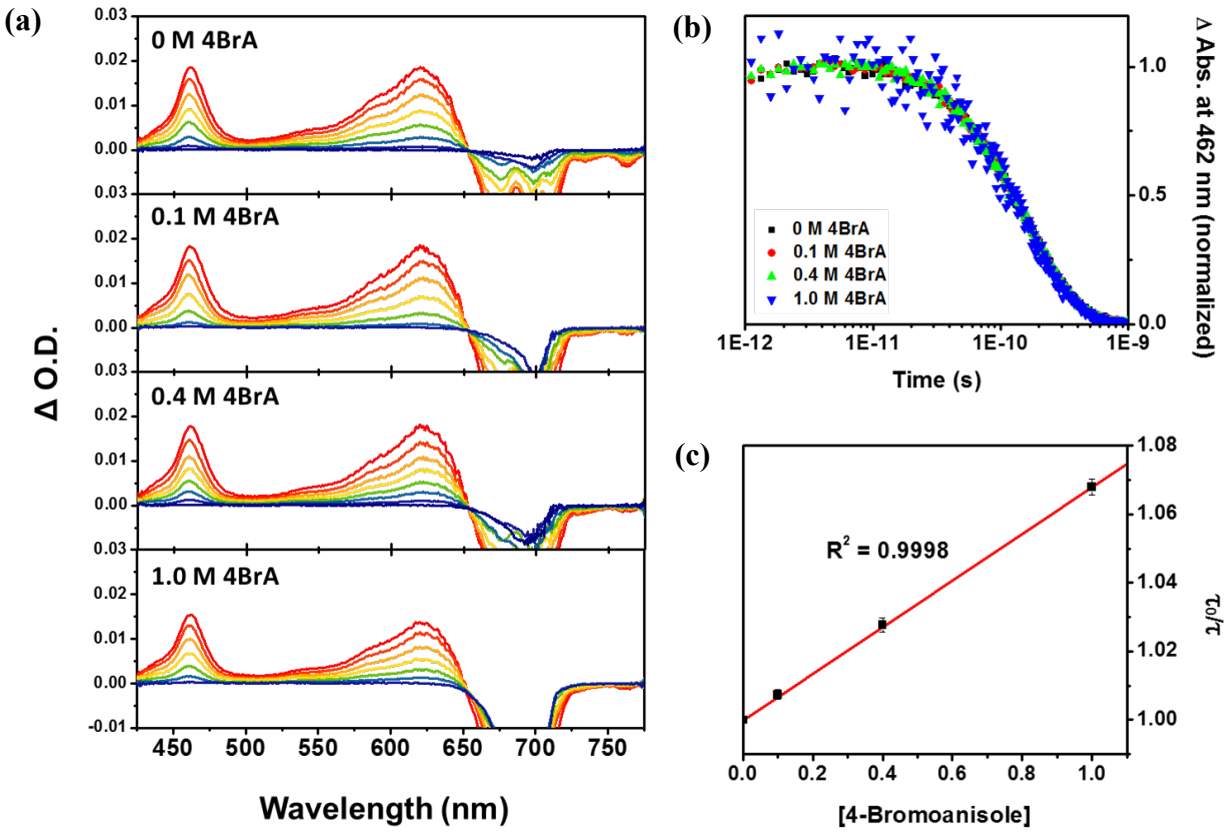

Figure S12. (a) Transient absorption spectra of 60 μM $PDI^{-\bullet}$ with 0 ~ 1.0 M of 4-bromoanisole in DMF. (b) Normalized kinetic traces at 462 nm of 60 μM $PDI^{-\bullet}$ with various concentration of 4-bromoanisole in DMF. (c) Stern-Volmer plot for the lifetime quenching of $PDI^{-\bullet}$ with various concentration of 4-bromoanisole in DMF.

3.13 Iodobenzene

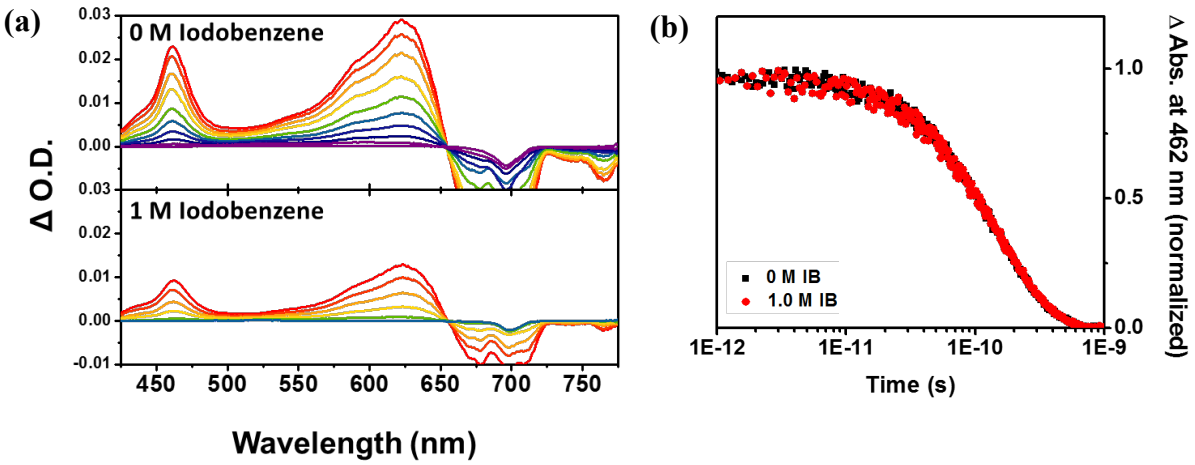

Figure S13. (a) Transient absorption spectra of 60 μM $PDI^{-\bullet}$ with 0, 1.0 M of iodobenzene in DMF. (b) Normalized kinetic traces at 462 nm of 60 μM $PDI^{-\bullet}$ with various concentration of iodobenzene in DMF. Note that the Stern-Volmer plot is not shown since there is no quenching observed up to 1.0 M concentration.

3.14 Benzonitrile

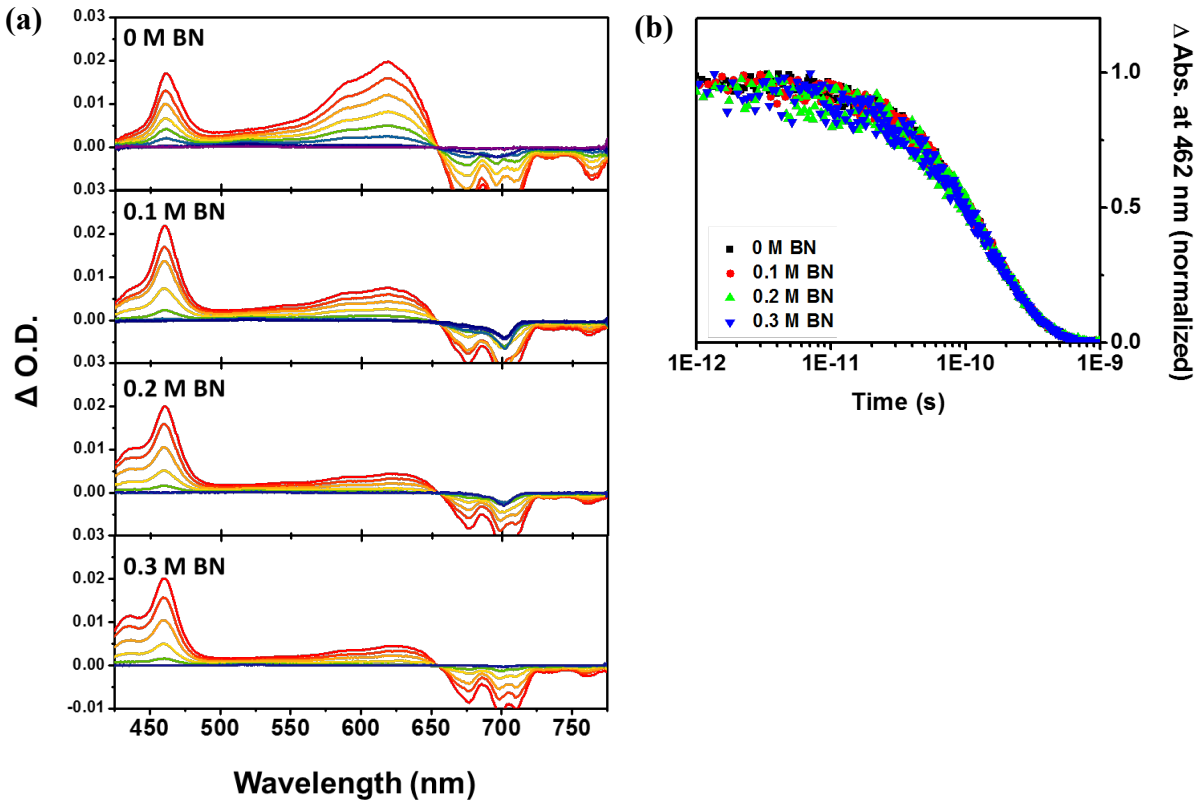

Figure S14. (a) Transient absorption spectra of 60 μM $PDI^{-\bullet}$ with 0 ~ 0.3 M of benzonitrile in DMF. (b) Normalized kinetic traces at 462 nm of 60 μM $PDI^{-\bullet}$ with various concentration of benzonitrile in DMF. Note that the Stern-Volmer plot is not shown since there is no quenching observed up to 0.3 M concentration.

3.15 Bromobenzene

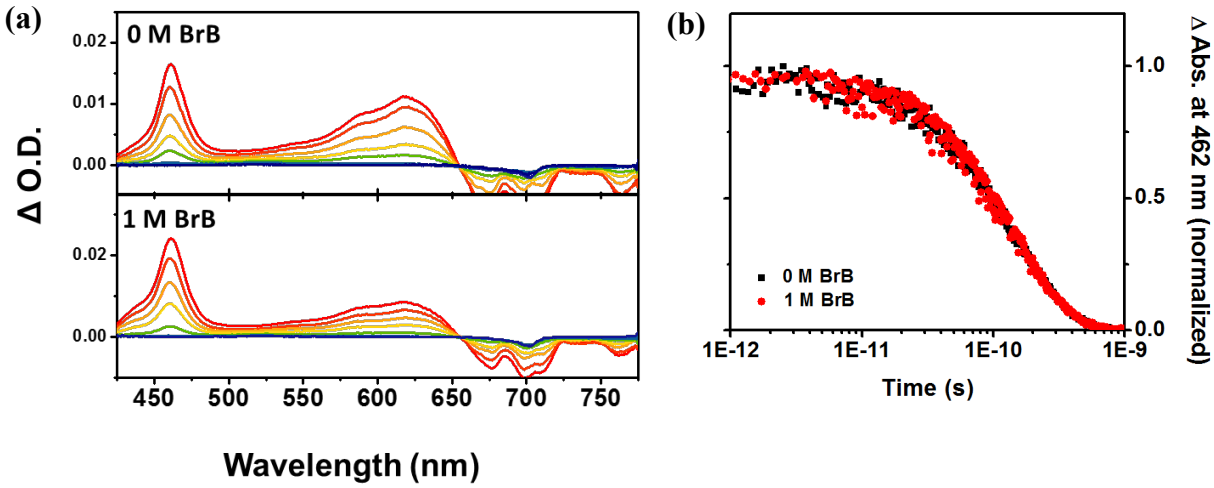

Figure S15. (a) Transient absorption spectra of 60 μM $PDI^{-\bullet}$ with 0, 1.0 M of bromobenzene in DMF. (b) Normalized kinetic traces at 462 nm of 60 μM $PDI^{-\bullet}$ with various concentration of bromobenzene in DMF. Note that the Stern-Volmer plot is not shown since there is no quenching observed up to 1.0 M concentration.

4. DARK REACTION OF $PDI^{-\bullet}$ IN THE PRESENCE OF QUENCHERS

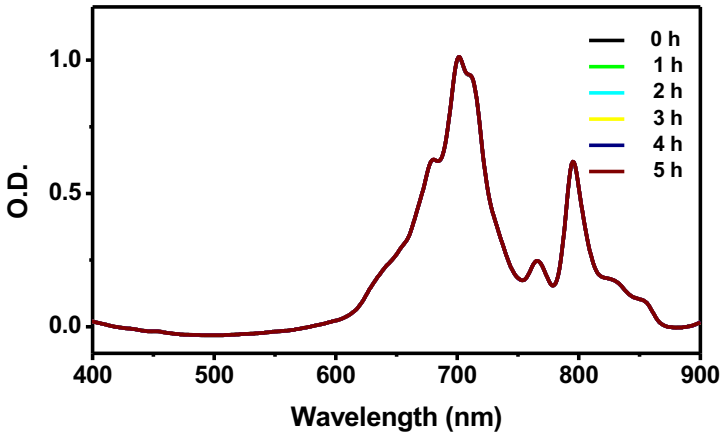

Figure S16. Change in the absorption spectrum of PDI (60 μM) and TDAE (60 μM) in DMF in dark conditions.

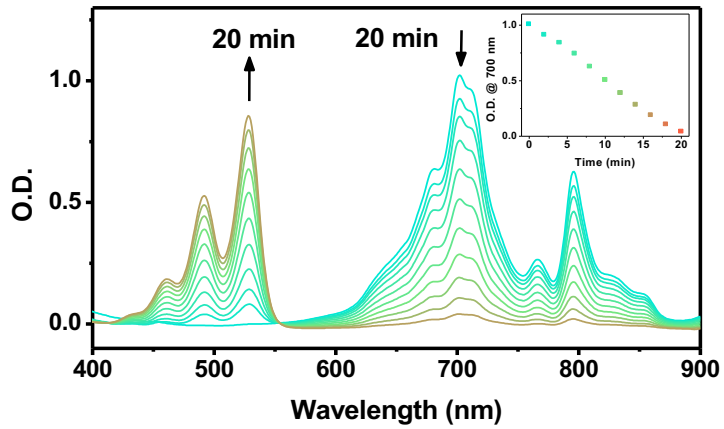

Figure S17. Change in the absorption spectrum of PDI (60 μM), TDAE (60 μM) and 4-iodobenzaldehyde (0.5 M) in DMF in dark conditions. E^{o} = -1.68 V vs. SCE

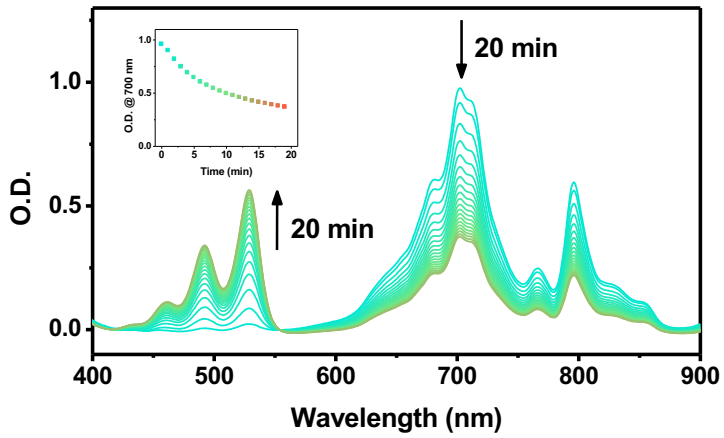

Figure S18. Change in the absorption spectrum of PDI (60 μM), TDAE (60 μM) and 3-iodobenzaldehyde (0.5 M) in DMF in dark conditions. E^o = -1.72 V vs. SCE

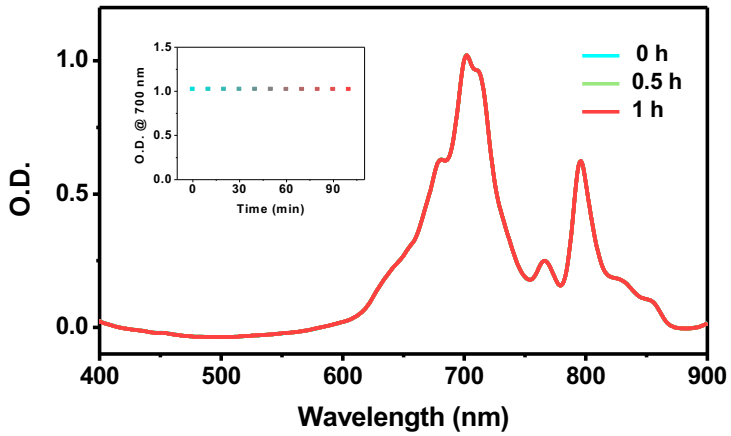

Figure S19. Change in the absorption spectrum of PDI (60 μM), TDAE (60 μM) and 4-bromobenzaldehyde (0.5 M) in DMF in dark conditions. E^o = -1.76 V vs. SCE

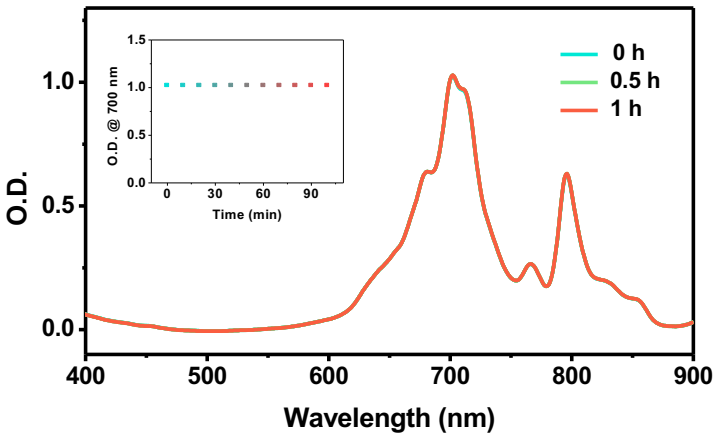

Figure S20. Change in the absorption spectrum of PDI (60 μM), TDAE (60 μM) and 4-bromoacetophenone (0.5 M) in DMF in dark conditions. E^o = -1.84, 1.89 V vs. SCE

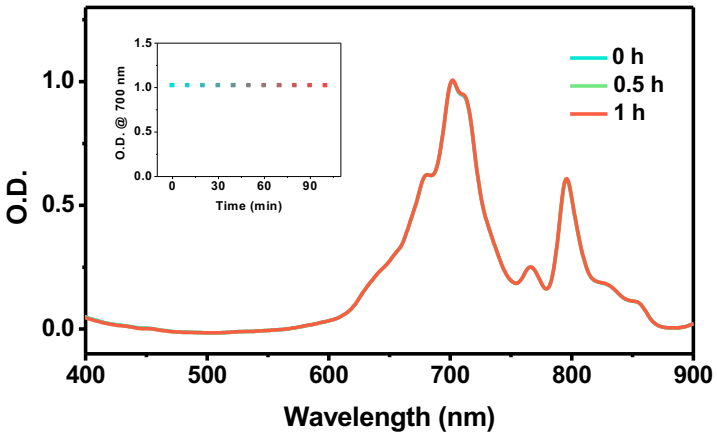

Figure S21. Change in the absorption spectrum of PDI (60 μM), TDAE (60 μM) and 4-chlorobenzaldehyde (0.5 M) in DMF in dark conditions. E^o = -1.85 V vs. SCE

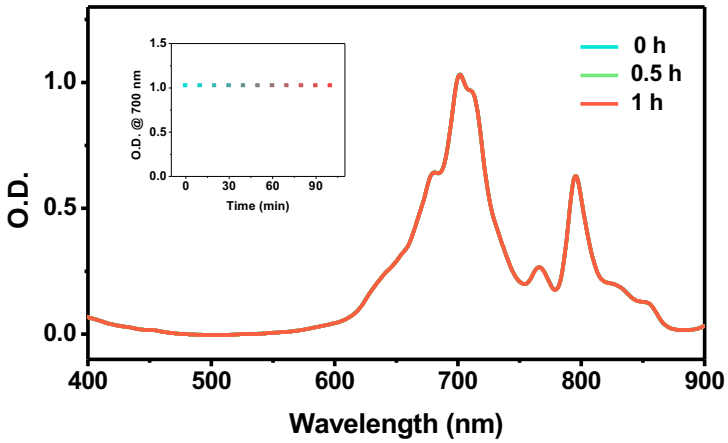

Figure S22. Change in the absorption spectrum of PDI (60 µM), TDAE (60 µM) and 2-chloro-4-(trifluoromethyl)pyridine (0.5 M) in DMF in dark conditions. E^o ~ -2.2 V vs. SCE

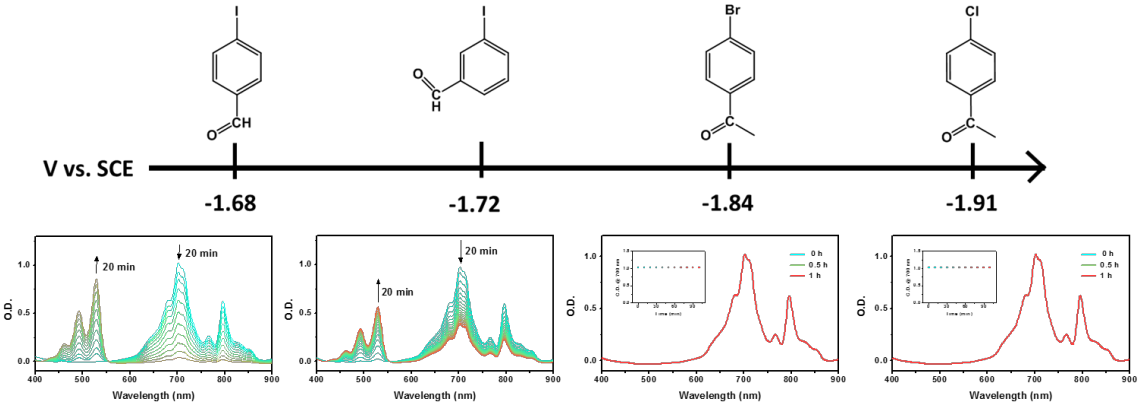

Figure S23. Change in absorption spectra of PDI (60 µM) with TDAE (60 µM) in the presence of four different aryl quenchers (0.5 M) of increasingly negative reduction potentials while isolated from light exposure.

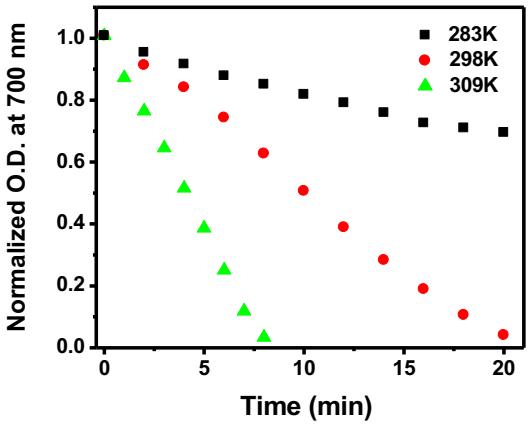

Figure S24. Change of absorption at 700 nm of PDI radical anion (60 μM) in the presence of 4-iodobenzadehyde (0.5 M) at three different temperatures in the dark.

5. QUANTITATIVE REDUCTION OF PDI BY TDAE

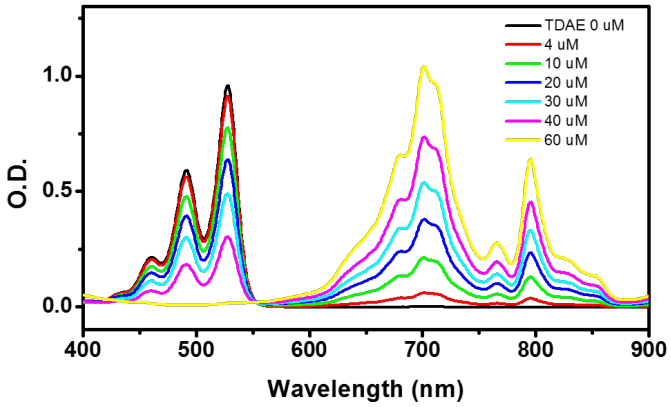

Figure S25. Absorption spectra of PDI (60 μM) with increasing concentrations of TDAE (0 to 60 μM) in DMF.

6. REFERENCES

(1) Balzani, V.; Bolletta, F.; Scandola, F., Vertical and "Nonvertical" Energy Transfer Processes. A General Classical Treatment. *J. Am. Chem. Soc.* **1980,** *102*, 2152-2163.

(2) Wang, Y; Schanze, K. S., Intramolecular Energy Transfer in (Diamine)$Re^{I}(CO)_3$-[CpM^{II}(Arene)] Dimers. *Inorg. Chem.* **1994,** *33*, 1354-1362.

(3) Cavalheiro, C. C. S.; Torraca, K. E.; Schanze, K. S.; White, L. M., Photophysics and Photoredox Properties of the Tungsten Carbyne Complex Cp{$P(OPh)_3$(CO)W:CPh. *Inorg. Chem.* **1999,** *38*, 3254-3257.

(4) Chambers, J. Q.; Adams, R. N., Solvent Effects on the Visible Spectra of Nitrobenzene Anion Radicals. *Mol. Phys.* **1965,** *9*, 413-415.